Annu. Rev. Mater. Res. 2004. 34:247–78
doi: 10.1146/annurev.matsci.34.040203.114607

First published online as a Review in Advance on March 16, 2004

UNUSUAL PROPERTIES AND STRUCTURE OF CARBON NANOTUBES

M.S. Dresselhaus,[1] G. Dresselhaus,[2] and A. Jorio[3]

[1]*Department of Electrical Engineering and Computer Science and Department of Physics, Massachusetts Institute of Technology, Cambridge, Massachusetts 02139-4307; email: millie@mgm.mit.edu*

[2]*Francis Bitter Magnet Laboratory, Massachusetts Institute of Technology, Cambridge, Massachusetts 02139-4307; email: gene@mgm.mit.edu*

[3]*Departamento de Física, Universidade Federal de Minas Gerais, Belo Horizonte-MG, 30123-970 Brazil; email: adojorio@fisica.ufmg.br*

Key Words nanotube structure, electronic properties, optical properties, phonon properties, mechanical properties, thermal properties, Raman spectroscopy, single nanotube spectroscopy

■ **Abstract** The unusual structure and properties of carbon nanotubes are presented, with particular reference to single-wall nanotubes (SWNTs) and nanotube properties that differ from those of their bulk counterparts. The atomic structure; electronic structure; and vibrational, optical, mechanical, and thermal properties are discussed, with reference made to nanotube junctions, nanotube filling, and double-wall nanotubes (DWNTs). Special attention is given to resonance Raman spectroscopy at the single nanotube level. The status of current research in this field is assessed and opportunities for future research are identified.

INTRODUCTION

The very small size of carbon nanostructures, their many unique physical phenomena, and simplicity in having only one chemical element, which allows physical properties to be calculated in detail for comparison with experiment, combine to give carbon nano-structures a special role in nanoscience. These systems provided numerous examples of theoretical predictions, often made before the experiments were done, and then the theories were tested in detail and improved once experimental results became available. Because of their unique properties, carbon nanostructures, and carbon nanotubes in particular, have many potential applications, and some of these could have significant impact on grand challenges of the twenty-first century.

At this early stage in nanoscience development, model systems pertinent at the small length scales that define nanoscience (lengths less than 30 nm) and where quantum effects are dominant are needed. The smaller the systems, the more likely

it is that quantum effects will play an increasingly important role. Because carbon nanotubes are found down to length scales of 0.4 nm, which is very small even in the realm of nanostructures, the structure and properties of carbon nanotubes are of particular interest. Model systems at the nanoscale are especially important for providing new ideas and concepts for what may be possible for more complex systems of small size. Complex systems are becoming of increasing interest now that we have calculational capabilities to handle detailed simulations for such systems. One of the grand challenges of the next few decades will be to advance the frontiers of nanoscience knowledge, to discover new exciting nanoscale phenomena, to develop new interesting materials systems, and to apply these advances toward addressing the societal challenges of the next generation. These challenges include producing the next generation of electronic and optoelectronic devices, bridging the gap between the inorganic world and that of living systems, and contributing new materials and technologies that can be utilized in gaining sustainable energy security for a growing worldwide population.

Carbon nanotubes are tubular structures typically of nanometer diameter and many microns in length. They are unusual because of their very small diameters, which can be as small as 0.4 nm and contain only 10 atoms around the circumference, and because the tubes can be only one atom in thickness. The aspect (length/diameter) ratio can be very large (greater than 10^4), thus leading to a prototype one-dimensional system. These structures were first observed by Endo in connection with synthesizing vapor-grown carbon fibers of increasingly smaller diameters (1) and by Iijima (2) in the soot produced in the arc-discharge synthesis of fullerenes, thereby attracting much attention to this work. The early structures were all of the multiwall morphology, consisting of coaxial cylinders arranged in a "Russian doll" configuration. The name multiwall nanotube (MWNT) is restricted to nanostructures with outer diameters of less than 15 nm, above which the structures are called carbon nanofibers and possess properties somewhere between carbon fibers and MWNTs (3). Because of the many interesting and often unexpected properties that carbon nanotubes exhibit, they have been extensively studied in the past decade, both in terms of the fundamental nanoscience revealed by these nanostructures and their potential for device applications.

The widespread recognition that MWNTs with very large aspect ratios could be synthesized led to consideration of the properties of the basic building blocks of the MWNTs, namely, a single cylinder with one atom thickness in the radial direction, later called a single-wall carbon nanotube (SWNT). The remarkable electronic properties calculated for these SWNTs [they could be either semiconducting or metallic depending on their geometry (4–6), as described below] attracted much interest. As a result of this stimulating environment, shortly after the 1991 paper of Iijima on MWNTs (2), SWNTs with small ($\sim$1 nm) and uniform diameters were synthesized in 1993 using arc-discharge methods with transition metal catalysts (7, 8). Crystalline ropes of SWNTs, with each rope containing tens to hundreds of tubes of approximately the same diameter closely packed into a triangular lattice, were synthesized in this early work. Subsequently, SWNTs have been synthesized

by a variety of methods, including arc-discharge, laser ablation, and vapor phase methods; within a few years, the synthesis technology had progressed to the point that sufficient amounts of SWNT samples could be provided for study of their fundamental properties (9). As in other fields of nanoscience, carbon nanotubes have provided, and continue to provide, a wonderful opportunity for the fruitful interaction between experiment, theory, and simulation, as is evident from the references cited within this review.

In this review, we first briefly summarizes the structure and notation used to describe carbon nanotubes. The next section is devoted to the electronic properties of SWNTs and how these properties are related to their geometry and structure. The influence of structural defects, such as pentagons and heptagons, is also discussed, as is the possibility of fabricating nanotube-based junctions of different geometries and their implications on nano-electronics. Then vibrational properties of nanotubes are reviewed, starting with the vibrational modes of SWNTs, particularly, how they are related to (and in what way they differ from) those of graphite. Raman spectroscopy of nanotubes is discussed in some detail, as this technique has been extensively used to probe the vibrational properties of nanotubes. The section on photophysics discusses the achievements of using light to study carbon nanotubes in the context of nanotube photophysics. We further discuss the exceptional mechanical and thermal properties of carbon nanotubes, and these exceptional properties are related to the strong in-plane carbon-carbon bonds, probably being the strongest atomic bonds found in nature. Filled SWNTs and double wall nanotubes (DWNTs) are examined, and we conclude with remarks about the many unanswered issues about nanotubes waiting to be resolved, as well as giving an outlook on future developments in this field.

STRUCTURE AND NOTATION

This section provides a brief introduction to the unusual structural properties of SWNTs, emphasizing their unique one-dimensional attributes that set them apart from other materials systems.

A SWNT can be described as a single layer of a graphite crystal rolled up into a seamless cylinder, one atom thick, usually with a small number (perhaps 10–40) of carbon atoms along the circumference and a long length (microns) along the cylinder axis (11). A carbon nanotube is specified by the chiral vector $\mathbf{C}_h$,

$$\mathbf{C}_h = n\mathbf{a}_1 + m\mathbf{a}_2 \equiv (n, m), \qquad 1.$$

which is often described by the pair of indices (n, m) that denote the number of unit vectors $n\mathbf{a}_1$ and $m\mathbf{a}_2$ in the hexagonal honeycomb lattice contained in the vector $\mathbf{C}_h$. As shown in Figure 1, the chiral vector $\mathbf{C}_h$ makes an angle θ, the chiral angle, with the so-called zigzag or $\mathbf{a}_1$ direction. The vector $\mathbf{C}_h$ connects two crystallographically equivalent sites O and A on a two-dimensional graphene sheet where a carbon atom is located at each vertex of the honeycomb structure (12). The axis of the zigzag nanotube corresponds to $\theta = 0^\circ$, whereas the so-called

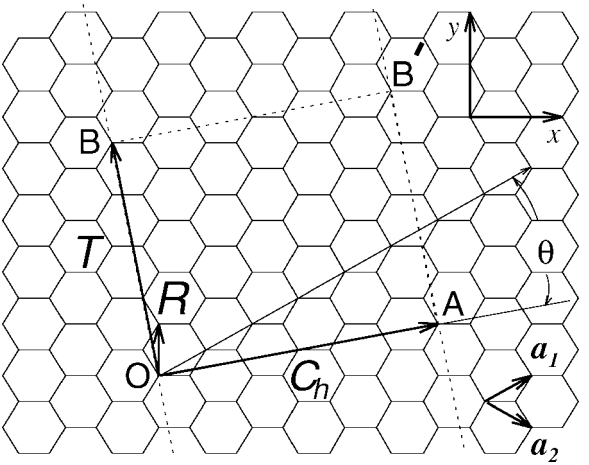

Figure 1 The unrolled honeycomb lattice of a nanotube. When we connect sites O and A, and sites B and B', a nanotube can be constructed. The vectors OA and OB define the chiral vector $\mathbf{C}_h$ and the translational vector $\mathbf{T}$ of the nanotube, respectively. The rectangle $OAB'B$ defines the unit cell for the nanotube. The figure is constructed for an $(n, m) = (4, 2)$ nanotube (10).

armchair nanotube axis corresponds to $\theta = 30^\circ$ and the nanotube axis for so-called chiral nanotubes corresponds to $0 < \theta < 30^\circ$. The seamless cylinder joint of the nanotube is made by joining the line AB' to the parallel line OB in Figure 1. The nanotube diameter d_t can be written in terms of the integers (n, m) as

$$d_t = C_h/\pi = \sqrt{3}a_{\mathrm{C-C}}(m^2 + mn + n^2)^{1/2}/\pi, \qquad 2.$$

where $a_{\mathrm{C-C}}$ is the nearest-neighbor C–C distance (1.421 Å in graphite), C_h is the length of the chiral vector $\mathbf{C}_h$, and the chiral angle θ is given by

$$\theta = \tan^{-1}[\sqrt{3}m/(m + 2n)]. \qquad 3.$$

Thus, a nanotube can be specified by either its (n, m) indices or equivalently by d_t and θ. Next, we define the unit cell $OBB'A$ of the one-dimensional nanotube in terms of the unit cell of the two-dimensional honeycomb lattice defined by the vectors $\mathbf{a}_1$ and $\mathbf{a}_2$ (Figure 1).

In Figure 2, we show (a) the unit cell in real space and (b) the Brillouin zone in reciprocal space of two-dimensional graphite as a dotted rhombus and a shaded hexagon, respectively, where $\mathbf{a}_1$ and $\mathbf{a}_2$ are basis vectors in real space and $\mathbf{b}_1$ and $\mathbf{b}_2$ are reciprocal lattice basis vectors. In the x, y coordinates shown in Figure 2, the real space basis vectors $\mathbf{a}_1$ and $\mathbf{a}_2$ of the hexagonal lattice are expressed as $\mathbf{a}_1 = (\sqrt{3}a/2, a/2)$ and $\mathbf{a}_2 = (\sqrt{3}a/2, a/2)$, where $a = |\mathbf{a}_1| = |\mathbf{a}_2| = 1.42 \times \sqrt{3} = 2.46$ Å is the lattice constant of a graphene or two-dimensional graphite layer.

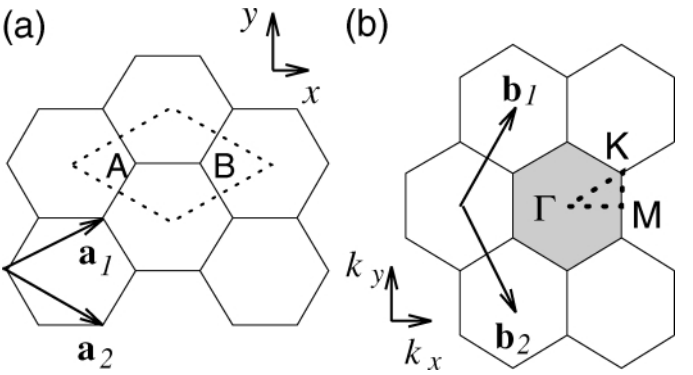

Figure 2 (*a*) The unit cell, containing sites A and B where carbon atoms are located, and (*b*) the Brillouin zone of a graphene or two-dimensional graphite layer are shown as the dotted rhombus and the shaded hexagon, respectively. $\mathbf{a}_i$ and $\mathbf{b}_i$ ($i = 1, 2$) are basis vectors and reciprocal lattice vectors, respectively. The high symmetry points, Γ, *K*, and *M* are indicated (13).

Correspondingly, the basis vectors $\mathbf{b}_1$ and $\mathbf{b}_2$ of the reciprocal lattice are given by $\mathbf{b}_1 = (2\pi/\sqrt{3}a, 2\pi/a)$ and $\mathbf{b}_2 = (2\pi/\sqrt{3}a, -2\pi/a)$, corresponding to the graphene lattice constant of $4\pi/\sqrt{3}a$ in reciprocal space. The direction of the basis vectors $\mathbf{b}_1$ and $\mathbf{b}_2$ of the reciprocal hexagonal lattice are rotated by 30° from the basis vectors $\mathbf{a}_1$ and $\mathbf{a}_2$ of the hexagonal lattice in real space, as shown in Figure 2.

To define the unit cell for the one-dimensional nanotube, we define the vector *OB* in Figure 1 as the shortest repeat distance along the nanotube axis, thereby defining the translation vector $\mathbf{T}$,

$$\mathbf{T} = t_1\mathbf{a}_1 + t_2\mathbf{a}_2 \equiv (t_1, t_2), \qquad 4.$$

where the coefficients t_1 and t_2 are related to (n, m) by

$$\begin{aligned} t_1 &= (2m + n)/d_R \\ t_2 &= -(2n + m)/d_R, \end{aligned} \qquad 5.$$

where d_R is the greatest common divisor of $(2n + m, 2m + n)$ and is given by

$$d_R = \begin{cases} d & \text{if} \quad n - m \text{ is not a multiple of } 3d \\ 3d & \text{if} \quad n - m \text{ is a multiple of } 3d, \end{cases} \qquad 6.$$

where d is the greatest common divisor of (n, m). The magnitude of the translation vector $T = |\mathbf{T}|$ is $|\mathbf{T}| = \sqrt{3}L/d_R$, where L is the length of the chiral vector $C_h = \pi d_t$ and d_t is the nanotube diameter. The unit cell of the nanotube is defined as the area delineated by the vectors $\mathbf{T}$ and $\mathbf{C}_h$. The number of hexagons, N, contained within the one-dimensional unit cell of a nanotube is determined by the integers (n, m) and is given by

$$N = 2(m^2 + n^2 + nm)/d_R. \quad 7.$$

The addition of a single hexagon to the honeycomb structure in Figure 1 corresponds to the addition of two carbon atoms. Assuming a value $a_{C-C} = 0.142$ nm on a carbon nanotube, we obtain $d_t = 1.36$ nm and $N = 20$ for a (10,10) nanotube. Because the real-space unit cell is much larger than that for a two-dimensional graphene sheet, the one-dimensional BZ for the nanotube is much smaller than the BZ for a single two-atom graphene two-dimensional unit cell. Because the local crystal structure of the nanotube is so close to that of a graphene sheet, and because the BZ is small, BZ-folding techniques have been commonly used to obtain approximate electron and phonon dispersion relations for carbon nanotubes with specific (n, m) geometrical structures.

Whereas the lattice vector $\mathbf{T}$ given by Equation 4 and the chiral vector $\mathbf{C}_h$ given by Equation 1 determine the unit cell of the carbon nanotube in real space, the corresponding vectors in reciprocal space are the reciprocal lattice vectors $\mathbf{K}_2$ along the nanotube axis and $\mathbf{K}_1$ in the circumferential direction, which gives the discrete k values in the direction of the chiral vector $\mathbf{C}_h$. The vectors $\mathbf{K}_1$ and $\mathbf{K}_2$ are obtained from the relation $\mathbf{R}_i \cdot \mathbf{K}_j = 2\pi\delta_{ij}$, where $\mathbf{R}_i$ and $\mathbf{K}_j$ are the lattice vectors in real and reciprocal space, respectively, and $\mathbf{K}_1$ and $\mathbf{K}_2$ therefore satisfy the relations

$$\mathbf{C}_h \cdot \mathbf{K}_1 = 2\pi, \quad \mathbf{T} \cdot \mathbf{K}_1 = 0,$$
$$\mathbf{C}_h \cdot \mathbf{K}_2 = 0, \quad \mathbf{T} \cdot \mathbf{K}_2 = 2\pi. \quad 8.$$

From Equation 8 it follows that $\mathbf{K}_1$ and $\mathbf{K}_2$ can be written as

$$\mathbf{K}_1 = \frac{1}{N}(-t_2\mathbf{b}_1 + t_1\mathbf{b}_2), \quad \mathbf{K}_2 = \frac{1}{N}(m\mathbf{b}_1 - n\mathbf{b}_2), \quad 9.$$

where $\mathbf{b}_1$ and $\mathbf{b}_2$ are the reciprocal lattice vectors of a two-dimensional graphene sheet given above. The N wave vectors $\mu\mathbf{K}_1$ ($\mu = 0, \cdots, N-1$) give rise to N discrete k vectors in the circumferential direction. For each of the μ discrete values of the circumferential wave vectors, a one-dimensional electronic energy band appears, whereas each μ gives rise to six branches in the phonon dispersion relations. Because of the translational symmetry of $\mathbf{T}$, there are continuous wave vectors in the direction of $\mathbf{K}_2$ for a carbon nanotube of infinite length. However, for a nanotube of finite length L_t, the spacing between wave vectors is $2\pi/L_t$, and quantum effects associated with the finite nanotube length have been observed experimentally (14).

ELECTRONIC PROPERTIES OF CARBON NANOTUBES AND JUNCTIONS

The nanometer dimensions of the carbon nanotubes together with the unique electronic structure of a two-dimensional graphene sheet make the electronic properties of these one-dimensional carbon nanotube structures highly unusual. The aim of the present section is to review the relation between the atomic structure and the

electronic and transport properties of SWNTs. The rich interplay between the structural and electronic properties of carbon nanotubes gives rise to new physical phenomena and the possibility of novel nanoscale device applications.

As shown in the previous section, a SWNT is geometrically just a rolled up graphene strip. Its structure can be specified or indexed by its circumferential periodicity and its chiral vector ($\vec{C}_h$) in terms of a pair of integers (n, m). Early theoretical calculations (5, 6, 13) have shown that the electronic properties of the carbon nanotubes are very sensitive to their geometric structure. Although graphene is a zero-gap semiconductor, theory has predicted that carbon nanotubes can be either metals or semiconductors with different size energy gaps, depending very sensitively on the diameter and helicity of the tubes, i.e., on the indices (n, m). The physics behind this sensitivity of the electronic properties of carbon nanotubes to their structure can be understood within a zone-folding picture. The electronic structure of the two-dimensional graphene layer near the Fermi energy is given by an occupied π band and an empty π^* band. These two bands have linear dispersion in $E(k)$ near the K point and, as shown in Figure 3, meet at the Fermi energy, which goes through at the K point in the BZ, thus identifying graphite as a zero-gap semiconductor. The Fermi surface of an ideal graphite sheet consists of the three corner K points alternating with the three corner K' points. When forming a tube, owing to the periodic boundary conditions imposed in the circumferential direction, only a certain set of $\vec{k}$ states of the planar graphite sheet

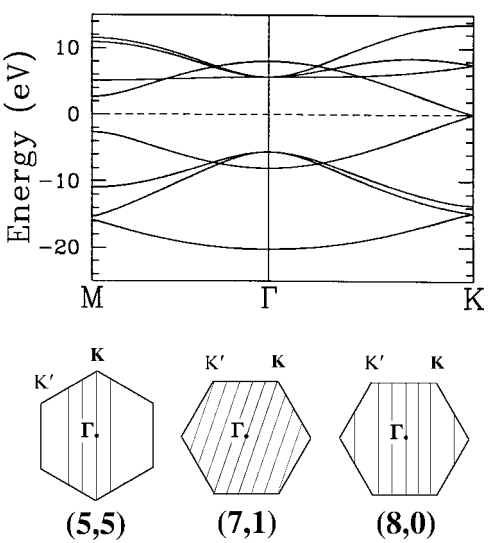

Figure 3 (*Top*) Tight-binding electronic band structure of graphene (a single basal plane of graphite) showing the Γ, *M*, and *K* high symmetry points. (*Bottom*) Allowed $\vec{k}$-vectors of the (5,5), (7,1), and (8,0) tubes (*solid cutting lines*) mapped onto the two-dimensional graphene Brillouin zone.

is allowed. The allowed set of k's, indicated by the cutting lines shown in the lower part of Figure 3, depends on the diameter and helicity of the SWNT (15). Whenever the allowed ks include the K (or K') point, the system is a metal with a nonzero density of states at the Fermi level, resulting in a one-dimensional metal with two bands showing a linear dispersion E versus k dependence. When the K point is not one of the allowed states, the system is a the semiconductor with an energy gap that increases as the tube diameter decreases. It is important to note that the states near the Fermi energy for both metallic and semiconducting tubes are all from states near the K or K' points, and hence their transport and other electronic properties are related to the properties of the states on the allowed cutting lines. For example, the conduction band and valence bands of a semiconducting carbon nanotube come from states along the line closest to the K point.

SWNTs are exceptional materials insofar as they can be metallic or semiconducting in accordance with the following rules: (n, n) tubes are metals; (n, m) tubes with $n - m = 3j$, where j is a nonzero integer, are very tiny-gap semiconductors; and all SWNTs with $n - m = 3j \pm 1$ are large-gap ($\sim$1.0 eV for $d_t \sim 0.7$ nm) semiconductors. Strictly within the zone-folding scheme, the $n - m = 3j$ tubes would all be metals, but because of tube curvature effects, a tiny band gap opens up when $j \neq 0$ (Figure 4). Hence, carbon nanotubes come in three varieties: large-gap, tiny-gap, and zero-gap systems. The (n, n) tubes, also known as armchair tubes, are always metallic within the single-electron picture, independent of curvature, because of their symmetry (Figure 4). As the tube diameter d_t increases, the band gaps of the large-gap and tiny-gap varieties decrease with a $1/d_t$ and $1/d_t^2$ dependence, respectively. Thus, for most experimentally observed carbon nanotubes, the gap in the tiny-gap variety, which arises from curvature effects, would be so small that, for most practical purposes, all the $n - m = 3j$ tubes can be considered as metallic at room temperature because their thermal energy is sufficient to excite electrons from the valence to the conduction band. Thus, in Figure 3 a (7,1) tube would be metallic, whereas a (8,0) tube would be semiconducting; the (5,5) armchair tube would always be metallic. Such a zone-folding picture, based on the tight-binding approach (5, 6, 13), is expected to be valid for larger diameter tubes ($d_t > 1$ nm), and this has been experimentally confirmed (16).

Ab initio pseudopotential local density functional (LDA) calculations (18, 19) indeed revealed that sufficiently strong hybridization effects between σ and π states can occur through tube curvature effects in small-diameter nanotubes, and these hybridization effects significantly alter their electronic structure. For example, the (5,0) tube, which is predicted to be semiconducting in the zone-folding scheme, has been shown to be metallic by ab initio calculations (20, 21). Unusual properties have also been found in ultra-small diameter SWNTs (diameter approximately 0.4 nm). These ultra-small diameter SWNTs are produced experimentally by confining their synthesis to occur inside inert $AlPO_4$-5 zeolite channels (with an inner diameter of approximately 0.73 nm) (22), thus leading to a narrow-diameter SWNT distribution, restricted to only three possible SWNTs: (3,3), (4,2), and (5,0). These ultra-small diameter SWNTs have been reported to exhibit a variety

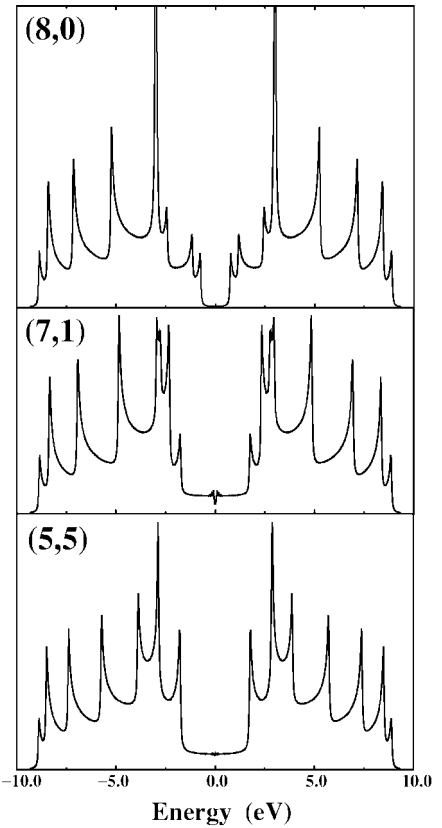

Figure 4 Electronic densities of states for (5,5), (7,1), and (8,0) nanotubes showing van Hove singularities characteristic of one-dimensional systems. The (5,5) armchair nanotube is metallic for symmetry reasons. The (7,1) chiral tube displays a tiny gap owing to curvature effects, but will display a metallic behavior at room temperature. The (8,0) zigzag tube is a large-gap semiconductor (17).

of unusual properties, such as superconductivity for an all-carbon system (23). Furthermore, the unit cell for such ultra-small diameter SWNTs is small enough to permit detailed and accurate ab initio calculations of their electronic structures (24, 25).

Many low-temperature transport measurements (14, 26–29) have been made on SWNTs in an attempt to understand their electronic properties. These results have been interpreted in terms of single-electron charging and resonant tunneling through the quantized energy levels of the nanotubes. In addition, there have also been atomic resolution low-temperature scanning tunneling microscopy (STM) and scanning tunneling spectroscopy (STS) studies, which directly probe the relationship between the structural and electronic properties of carbon nanotubes

(30, 31). From measurements of the orientation of the carbon rings relative to the nanotube axis and of the tube diameter d_t, the geometric structure of the nanotube was fully deduced. Measurement of the normalized conductance in the STS mode was then used to obtain the local density of states (LDOS), and the experimental results were in very good agreement with theoretical predictions.

However, carbon nanotubes often exhibit defects such as pentagons, heptagons, vacancies, or dopants that drastically modify their electronic properties. The electronic properties of defective nanotube-based structures are, of course, more complex than those for infinitely long, perfect nanotubes. The introduction of defects into the carbon network is thus an interesting way to tailor its intrinsic properties to create new potential nanodevices and to propose new potential applications for nanotubes in nano-electronics.

Because carbon nanotubes are metals or semiconductors, depending sensitively on their geometrical structures, they can be used to form metal-semiconductor, semiconductor-semiconductor, or metal-metal junctions. These junctions have great potential for applications because they are of nanoscale dimensions and are made entirely of a single chemical element. In constructing this kind of on-tube junction, the key is to join two half-tubes of different helicities seamlessly with each other, without too much cost in energy or disruption in structure. The introduction of pentagon-heptagon pair defects into the hexagonal network of a single carbon nanotube can change the helicity of the carbon nanotube and fundamentally alter its electronic structure (17, 32–35). Both the existence of such atomic-level structures and investigations of their respective electronic properties have already been carried out experimentally (36, 37).

The defects, however, must induce zero net curvature to prevent the tube from flaring or closing. The smallest topological defect with zero net curvature is a pentagon-heptagon pair, which can be treated as a single local defect because it creates only topological changes (but no net disclination). Such a 5/7 pair will create only a small local deformation in the width of the nanotube and may also generate a small change in the helicity, depending on its orientation in the hexagonal network.

Joining a semiconducting nanotube to a metallic one, using a pentagon-heptagon 5/7 pair incorporated in the hexagonal network can be the basis of a nanodiode (or molecular diode) for nano-electronics. An example of such a diode structure is the junction of a semiconducting (8,0) nanotube that has a 1.2 eV gap in the tight-binding approximation and a (7,1) tube that is a metal (although a small curvature-induced gap is present close to the Fermi energy). Nanotube junctions thus can behave as nanoscale metal-metal junctions, metal-semiconductor Schottky barrier junctions, or semiconductor heterojunctions with novel properties, and these different types of junctions can serve as building blocks for nanoscale electronic devices.

Recently, the electron beam of a transmission electron microscope has been used to irradiate nanostructures locally to introduce defects that can be useful for device applications. Covalently connected crossed SWNTs have thus been

created using electron beam welding at elevated temperatures (38, 39) to produce molecular junctions of various geometries ("X," "Y," and "T" junctions), and these junctions are found to be stable after the irradiation process. To study the relevance of some of these nanostructures, various models of ideal molecular junctions have been generated. The presence of heptagons plays a key role in the topology of nanotube-based molecular junctions. The flexibility of the nanoscale design and the availability of both semiconducting and metallic nanotubes enable a wide variety of configurations. Junctions between semiconducting and metallic nanotubes can act as diodes. Junctions between two crossed nanotubes can act as rectifiers, and Y-, T-, or X-junctions provide more exotic configurations for nanoscale devices. Although a number of early nanotube-based devices have already been demonstrated, the production and integration of nanotube components into reproducible device structures present many challenges. Several major steps toward nanotube-based circuitry have, however, been achieved: An array of field-effect transistors has been made by selectively burning-off metallic nanotubes in SWNT ropes (40), and field-effect transistors based on single nanotubes have been assembled by several research groups into the logic circuits that are building blocks of computers (40–42), showing promise for future developments in nanocircuitry.

PHONON PROPERTIES AND RAMAN SPECTROSCOPY OF CARBON NANOTUBES

Phonons denote the quantized normal mode vibrations that strongly affect many processes in condensed matter systems, including thermal, transport, and mechanical properties. Phonons play an important role as a carrier of thermal energy in thermal conduction processes and in thermodynamic properties, such as the heat capacity, and as an important scattering process for bringing electrons into equilibrium with the lattice in various electron transport phenomena, such as electrical conductivity, magneto-transport phenomena, and thermo-electricity. The vibrational spectra also determine the speed of sound, elastic properties of solids, and their mechanical properties. Phonons, through their interaction with electrons, can also mediate interactions and pairing between electrons, giving rise to superconductivity. These topics are particularly interesting in one-dimensional systems because of the van Hove singularities that one-dimensional systems exhibit in their density of states (see Figure 4). These phenomena are even more interesting in SWNTs, which allow these one-dimensional effects to be studied in detail.

Because a SWNT can be considered to be a two-dimensional graphene sheet that has been rolled up seamlessly, the electron dispersion relations of SWNTs are typically related to those of two-dimensional graphite (a graphene sheet), as is discussed above. A similar procedure is generally applied to obtain the phonon dispersion relations and phonon density of states for SWNTs from those of the two-dimensional graphene sheet (10), as is illustrated, respectively, in Figure 5*a*,*b* for a

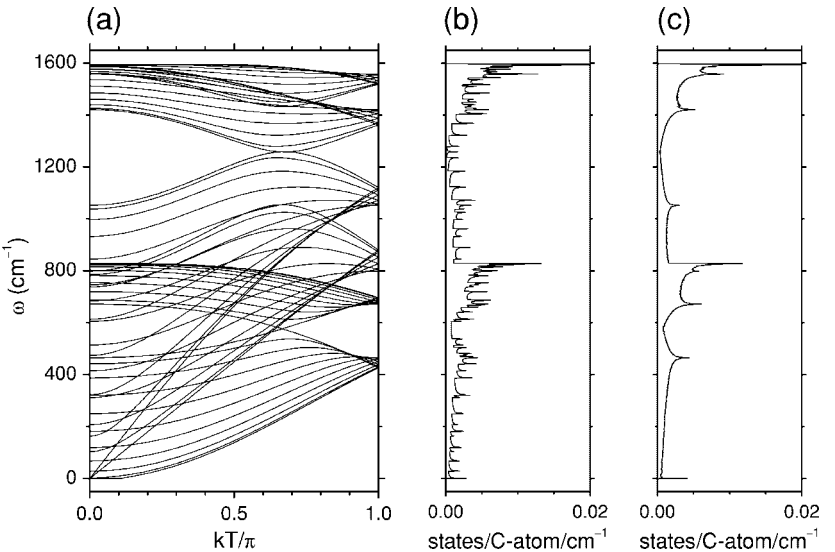

Figure 5 (*a*) The calculated phonon dispersion relations of an armchair carbon nanotube with $(n, m) = (10, 10)$. The number of degrees of freedom is 120 and the number of distinct phonon branches is 66 (10). (*b*) The corresponding phonon density of states for a (10,10) nanotube (43). (*c*) The corresponding phonon density of states for a two-dimensional graphene sheet (10).

(10,10) SWNT. The large amount of sharp structure in the phonon density of states in Figure 5*b* for the (10,10) SWNT reflects the many phonon branches and the one-dimensional nature of SWNTs relative to two-dimensional graphite. The phonon density of states for two-dimensional graphite shown in Figure 5*c* is obtained by summing the one-dimensional phonon density of states for many SWNTs (10, 43). In addition to the longitudinal acoustic (LA) and transverse acoustic (TA) modes, there are two acoustic twist modes for rigid rotation around the tube axis, which are important for heat transport and charge carrier scattering. Also important for coupling electrons to the lattice are the low-lying optical modes at the center of the BZ $q = 0$. These modes include one with E_2 symmetry expected at $\sim$17 cm^{-1} (the squash mode), one with E_1 symmetry expected at $\sim$118 cm^{-1}, and one with A symmetry (radial breathing mode, RBM) expected at $\sim$165 cm^{-1} for a (10,10) SWNT (10). Of these three low-energy phonon modes, it is only the RBM, where all the carbon atoms are vibrating in phase in the radial direction, that has been studied experimentally. The RBM is unique to SWNTs and does not occur in other carbon systems. The radial breathing mode has been of great importance in identifying the presence of SWNTs in samples containing other carbon materials and in determining SWNT diameters d_t, as discussed below, and measurements of the RBM have become a standard method used for the characterization of carbon nanotubes.

Raman Spectroscopy

The Raman spectra of SWNTs have been particularly valuable for providing detailed information on the vibrational modes of SWNTs (44), for characterizing SWNT samples (43, 45), and for revealing a variety of unique phenomena in one-dimensional systems (15, 46). The first report on the Raman spectra of SWNTs (45) showed that, despite the large number of branches in the SWNT phonon dispersion relations (see Figure 5*a*), the Raman spectra for a SWNT bundle (see Figure 6) only exhibit two dominant features, namely, the RBM out-of-plane vibrations, at 186 cm^{-1} for laser excitation energy $E_{laser} = 2.41$ eV and a SWNT diameter distribution of 1.36 ± 0.20 nm, and the tangential (in-plane vibrations) band in the range from 1520–1620 cm^{-1} (see Figure 6 inset). Because of the strong connection of this tangential band to the corresponding mode in two-dimensional graphite, this higher frequency band for SWNTs is commonly called the *G*-band. Other lower intensity features, discussed below, also provide important and unique information about SWNTs.

The strong and nonmonotonic dependence of the SWNT Raman spectra on the laser excitation energy E_{laser} established Raman scattering to be associated with a resonance process for the excitation laser energy E_{laser} with the optical transition energy E_{ii} between van Hove singularities in the valence band and conduction bands (see Figure 4) (45). Because of the very small diameters of SWNTs (~1 nm), the joint density of states for this optical process exhibits van Hove singularities

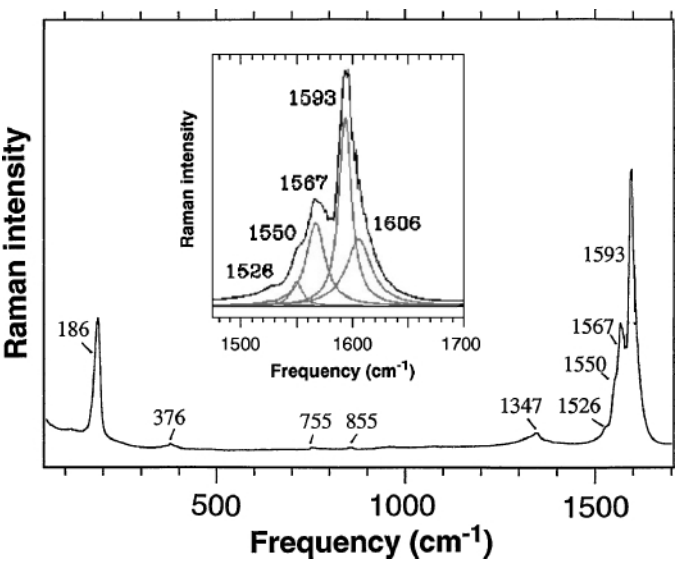

Figure 6 Experimental Raman spectrum taken with 514.5 nm (2.41 eV) laser excitation from a SWNT bundle sample with a diameter distribution $d_t = 1.36 \pm 0.20$ nm. The inset shows an expanded view of the spectra in the 1480–1700 cm^{-1} range (45).

with very large magnitudes (see Figure 4), giving rise to very large enhancements in Raman intensity and allowing the observation of spectra from one individual SWNT that is in strong resonance with E_{laser} (47).

Figure 6 indicates that the G-band feature for SWNTs consists of two features: one peaked at 1593 cm^{-1} (G^+) and the other peaked at 1567 cm^{-1} (G^-). The G^+ feature is associated with carbon atom in-plane vibrations along the nanotube axis, and its frequency ω_{G^+} is sensitive to charge transfer from dopant additions to SWNTs (up-shifts in ω_{G^+} for acceptors and downshifts for donors). In contrast, the G^- feature is associated with in-plane vibrations of carbon atoms along the circumferential direction of the nanotube, and its line-shape is highly sensitive to whether the SWNT is metallic (Breit–Wigner–Fano line-shape) or semiconducting (Lorentzian line-shape) (48, 49). Whereas the most intense peaks at 1593 cm^{-1} and 1567 cm^{-1} arise from phonons with A and E_1 symmetries, the smaller intensity features at 1526 cm^{-1} and 1606 cm^{-1} are associated with E_2 symmetry phonons. Phonons with A, E_1, and E_2 symmetries can be distinguished from one another by their behavior in polarization-sensitive Raman experiments (50, 51).

Also commonly found in the Raman spectra in SWNT bundles is the D-band feature with ω_D at 1347 cm^{-1} in Figure 6, stemming from the disorder-induced mode in graphite, and its second harmonic, the G'-band (not shown) occurring at $\sim 2\omega_D$, both associated with a double resonance process (52). Both the D-band and the G'-band are sensitive to the nanotube diameter and chirality and therefore have been very important in revealing much new physics about carbon nanotubes from single nanotube studies, as discussed below. Study of the D-band and G'-band features have been very important for studying trigonal warping effects in SWNTs and in quantitatively measuring the effect of trigonal warping on the dispersion relations for electrons (53, 54) and for phonons (55).

Returning to Figure 6, the weak feature at 116 cm^{-1} may be due to a low frequency E_1 symmetry SWNT mode that is not observed in graphite, whereas the mode at 376 cm^{-1} is likely to be the second harmonic of ω_{RBM}. The broad weak feature at 857 cm^{-1} is identified with the out-of-plane optical, transverse optical (TO) mode that is infrared (IR) active in two-dimensional graphite, whereas the feature at 1736 cm^{-1} is identified with its second harmonic. Both the 857 cm^{-1} and the 1736 cm^{-1} features are commonly seen in SWNT bundles and at the single nanotube level, and these features are attributed to a double resonance process (56). The intermediate frequency feature at 754 cm^{-1} is a very special mode that arises in nanotubes because of the special properties of one-dimensional phonons (C. Fantini et al. unpublished).

Because of the sharp van Hove singularities occurring in carbon nanotubes with diameters less than 2 nm (see Figures 4, 5), the Raman intensities for the resonance Raman process can be so large that it is possible to observe the Raman spectra from one individual SWNT (47), as shown in Figure 7, where the differences in the G-band spectra between semiconducting and metallic SWNTs can be seen at the single nanotube level. Because of the trigonal warping effect (54), every (n, m) carbon nanotube has a different electronic structure and therefore also

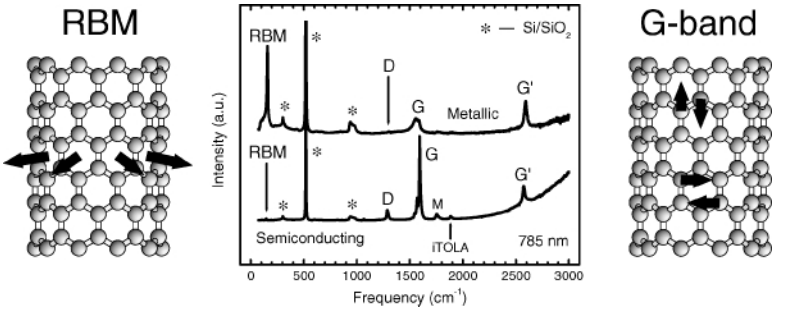

Figure 7 Raman spectra from a metallic (*top*) and a semiconducting (*bottom*) SWNT at the single nanotube level using 785 nm (1.58 eV) laser excitation, showing the radial breathing mode (RBM), *D*-band, *G*-band, and *G′*-band features, in addition to weak double resonance features associated with the M-band and the iTOLA second-order modes (56). Insets on the left and the right show atomic displacements associated with the RBM and *G*-band normal mode vibrations (15). The isolated carbon nanotubes are sitting on an oxidized silicon substrate that provides contributions to the Raman spectra, denoted by *, which are used for calibration purposes (47).

has a unique density of states (see Figure 4). Therefore, the energies E_{ii} of the van Hove singularities in the joint density of states for each SWNT are different, as shown in Figure 8, for all (n, m) nanotubes in the diameter range up to 3.0 nm and for E_{ii} up to 3.0 eV. In this so-called Kataura plot (Figure 8), we see that for small-diameter SWNTs ($d_t < 1.7$ nm) and for the first few electronic transitions for semiconducting and metallic SWNTs, the E_{ii} values are arranged in bands whose width is determined by the trigonal warping effect (54). A general chiral semiconducting SWNT will have van Hove singularities (vHSs) in the E_{11}^S, E_{22}^S, E_{33}^S,. . . bands, whereas a chiral metallic SWNT will have two vHSs in each of the E_{11}^M, E_{22}^M,. . . bands. The tight binding approximation provides quite reliable values for the E_{ii} energies for the vHSs for SWNTs with diameters in the 1.0–2.0 nm range (to an accuracy of better than 20 meV) (16). The Raman effect provides a determination of E_{ii} values, either by measurement of the relative intensities of the RBM for the Stokes (phonon emission) and anti-Stokes (phonon absorption) processes or by RBM-relative Raman intensity measurements for the Stokes process for many SWNTs (47, 60). The frequency of the RBM is used to determine the diameter of an isolated SWNT sitting on an oxidized Si surface using the relation ω_{RBM} (cm^{-1}) $= 248/d_t$ (nm), and from a knowledge of the (E_{ii}, d_t) values for an individual SWNT (Figure 8), the (n, m) indices for that SWNT can be determined from the Kataura plot. However, the linear relation $\omega_{\mathrm{RBM}} = 248/d_t$ seems not to apply in the case of very-small-diameter SWNTs (d_t below 1 nm), where both experimental results (16, 61) and ab initio calculations (62) show that the RBM frequency does not exhibit a simple dependence on d_t. For small-diameter SWNTs, the hexagons become distorted, and because this distortion depends on chiral angle, a θ dependence for ω_{RBM} is expected for small d_t SWNTs (62).

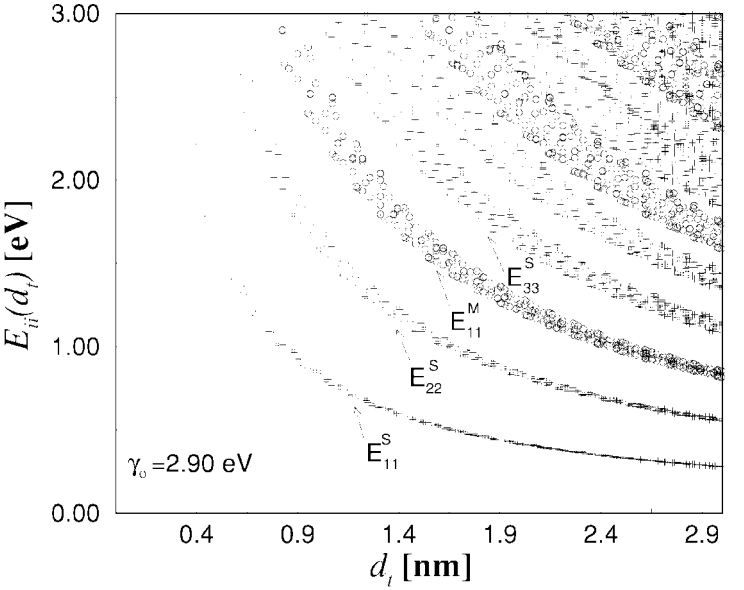

Figure 8 Calculated (58) energy separations E_{ii} between van Hove singularities i in the one-dimensional electronic density of states of the conduction and valence bands for all possible (n, m) values versus nanotube diameter in the range $0.5 \leq d_t \leq 3.0$ nm, using a tight-binding method with a value for the carbon-carbon energy overlap integral of $\gamma_0 = 2.9$ eV for making this plot (54, 59). Semiconducting (S) and metallic (M) nanotubes are indicated by crosses and open circles, respectively. The subscript $i = 1$ denotes the index of the lowest energy of a singularity in the joint density of states.

Systematic experimental work is still needed for determining the ω_{RBM} dependence on (d_t, θ) for small-diameter SWNTs. Whereas resonance Raman scattering is usually a sensitive spectroscopic technique, single nanotube spectroscopy shows how resonance Raman scattering spectra can be used on mesoscopic systems as a technique for structural determinations. Resonance Raman spectroscopy at the single nanotube level not only can determine the (n, m) indices from study of the RBM frequency and intensity, but studies of other features in the Raman spectra also provide valuable information not obtainable from SWNT bundles (60) or by using other characterization techniques.

Measurements on the G-band at the single nanotube level show that this feature is a first-order process, with the frequency ω_{G^+} essentially independent of d_t or chiral angle θ, while ω_{G^-} is only dependent of d_t and not on θ. Such diameter-dependent measurements can be done only at the single nanotube level, and the results can be used along with many other measurements to corroborate (n, m) assignments carried out on the basis of the RBM feature (47). Single nanotube measurements of the D-band and G'-band features show these features to be

connected to a double resonance process (63), with special properties associated with the van Hove singularities of the SWNTs (53, 64–66). Measurements of the D-band and the G'-band frequencies at the single nanotube level provide unique information on the chirality and diameter dependence of ω_D and $\omega_{G'}$ and can be used to measure the trigonal warping effect in the electron and phonon dispersion relations of SWNTs, providing information not readily available using other experimental techniques (60). Measurements of ω_D and $\omega_{G'}$ for special semiconducting SWNTs, where the incident photon is in resonance with one vHS (e.g., E_{44}^S) and the scattered photon is in resonance with another vHS (e.g., E_{33}^S) is a special Raman effect that can be observed for very special SWNTs. These observations are particularly useful for corroborating specific (n, m) assignments made by the RBM mode, as well as for corroborating the (n, m) assignment procedure itself (60).

The corresponding measurements for metallic SWNTs provide definitive information about the magnitude of the trigonal warping effect in the electronic structure of SWNTs because of the strong coupling of electrons and phonons under strong coupling conditions (53). Furthermore, changes in the Raman spectra can be used to probe and monitor structural modifications of the nanotube sidewalls that come from the introduction of defects and the attachment of different chemical species. The former effect can be probed through analysis of the disorder-induced Raman modes (e.g., the D-band assigned in Figure 7*b*) and the latter through the upshifts/downshifts observed in the various Raman modes owing to charge transfer effects (67). The ability to use a gate (68), an externally applied potential (P. Corio et al., unpublished), or a tunable laser (70; C. Fantini et al., unpublished) to move the vHS for an individual SWNT into and out of resonance with the laser offers great promise for detailed studies of the one-dimensional physics of SWNTs using resonance Raman spectroscopy.

Raman spectra of carbon nanotubes, particularly at the single nanotube level, have been especially rich. Because of the simplicity of the geometrical structure of nanotubes, detailed analysis of the Raman spectra has yielded much information about the phonon dispersion relations, such as information about their trigonal warping (55). This information was in fact not yet available for two-dimensional graphite, but could be studied in nanotubes because of their one-dimensionality. Thus, studies on carbon nanotubes are revealing much important information about the electrons and phonons in two-dimensional graphite through studies on carbon nanotubes at the single nanotube level, where the orientation of the wave vector can be explicitly probed, in contrast to the situation in two-dimensional graphite, which only allows measurements to be made as a function of the magnitude of the wave vector (55). For example, the trigonal warping of the phonon dispersion relations about the K (and K′) point of the BZ cannot be probed directly in graphite because k vectors in all directions are simultaneously probed, whereas for SWNTs, the unique vector along the tube axis is probed, allowing the anisotropy of the phonon dispersion relations to be directly probed in SWNTs and thereby related to the phonon dispersion in two-dimensional graphite (55). Furthermore, Raman studies at the single nanotube level have shown how phonon dispersion relations along

symmetry axes can be probed for nanoscale systems (71) for which conventional inelastic neutron scattering experiments (72) cannot be carried out.

PHOTOPHYSICS OF CARBON NANOTUBES

Together with resonance Raman spectroscopy, a variety of optical techniques, such as IR spectroscopy, absorption measurements, fast-optics, and photo-luminescence, have provided powerful means for identifying unusual properties associated with carbon nanotubes.

Near-IR spectroscopy can be used for a quantitative evaluation of the carbonaceous purity of bulk quantities of as-prepared SWNTs in a solution-phase (73), which is important for practical applications. Far-IR spectroscopy has been used to study electrons in SWNTs, giving information about plasmons and about the unusual tiny gaps occurring in quasimetallic SWNTs owing to curvature effects (74) (see above).

Time-domain photoelectron spectroscopy studies using fast-optics also provide information about electrons, such as the lifetime for the excited states and the strength of the electron-phonon coupling in SWNTs (see Figure 9). Experimental pump-probe results on SWNT bundles show that electron-phonon scattering is associated with a long scattering time of approximately 15 ps (76). The

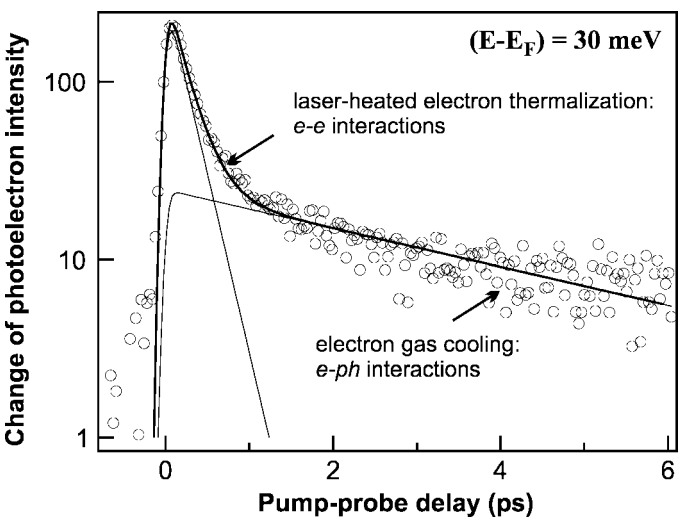

Figure 9 Time dependence of the photoelectron intensity during and after femtosecond laser generation of "hot" electrons in SWNT ropes (75). Electrons monitored by this trace are 30 meV above the Fermi level. The fast and slow components, respectively, correspond to internal thermalization of the laser-heated electron gas and to its equilibration with the lattice, i.e., by cooling.

lifetime of electrons excited to the π^* bands is found to decrease continuously from 130 fs at 0.2 eV down to less than 20 fs at energies above 1.5 eV with respect to the Fermi level (75, 77). Generally, the E_{ii} vHSs in the electronic joint density of states (JDOS) shown in Figure 8 are responsible for the unique optical properties observed in SWNTs. Owing to the diverging character of vHSs in these one-dimensional systems, one expects to find a very large resonant enhancement of the corresponding photophysical process, and such enhancement can be very strongly confined in energy, appearing almost as if the transitions to excited states were in a molecular system. The observed decrease in the lifetime of excited electrons as their energy increases relative to the Fermi level should lead to a significant lifetime-induced broadening of the characteristic vHSs in the density of states, so that optical effects related to the confinement of electrons into vHSs should be stronger for the lower energy vHSs in the JDOS.

Raman spectroscopy, optical absorption, and photoluminescence have all been used to determine E_{ii} energy values, which led to the development of theoretical models to describe the nanotube electronic structure for excited states. State-of-the-art optical measurements provide access to the electronic transition energies E_{ii} at the single nanotube level. Stokes versus anti-Stokes Raman signals at the isolated SWNT level with a single laser line allow the determination of E_{ii} within ± 10 meV precision for SWNTs sitting on a Si/SiO_2 substrate (43, 67, 78). The precision of this assignment using Stokes versus anti-Stokes Raman measurements depends on the determination of the shape of the resonance window (Raman intensity as a function of excitation laser energy E_{laser}). Resonance Raman experiments with a tunable laser system provide such a resonance window and give E_{ii} with high accuracy ($\sim \pm 3$ meV). The resonance window could change for samples with different environments (substrates) and sample preparation methods, and systematic work should be carried out to study these environmental factors and to increase the precision in the E_{ii} determination.

Optical absorption and emission measurements on carbon nanotube samples show peaks corresponding to E_{ii} values for individual (n, m) SWNTs, with linewidths of ~ 25 meV corresponding to the room temperature thermal energy (79–82). The observation of the E_{11}^S energy gap for semiconducting SWNTs is possible by measuring photoluminescence, and interesting three-dimensional plots can be constructed (see Figure 10) that show the spectral interdependence of the absorption and emission energies. The intense peaks, indicating strong optical absorption at a given E_{ii} and emission at E_{11}, are related to one specific (n, m) SWNT. The limitation for photoluminescence is related to systems where nonradiative electron-hole recombination readily occurs, so that light emission from metallic SWNTs or from SWNTs in bundles cannot be observed. For such samples, resonance Raman experiments could be alternatively used for E_{ii} determinations.

The accurate E_{ii} photophysical measurements at the single nanotube level made possible the determination of the inaccuracy of the simple nearest-neighbor tight binding (TB) model to describe the E_{ii} energies, as shown by different optical

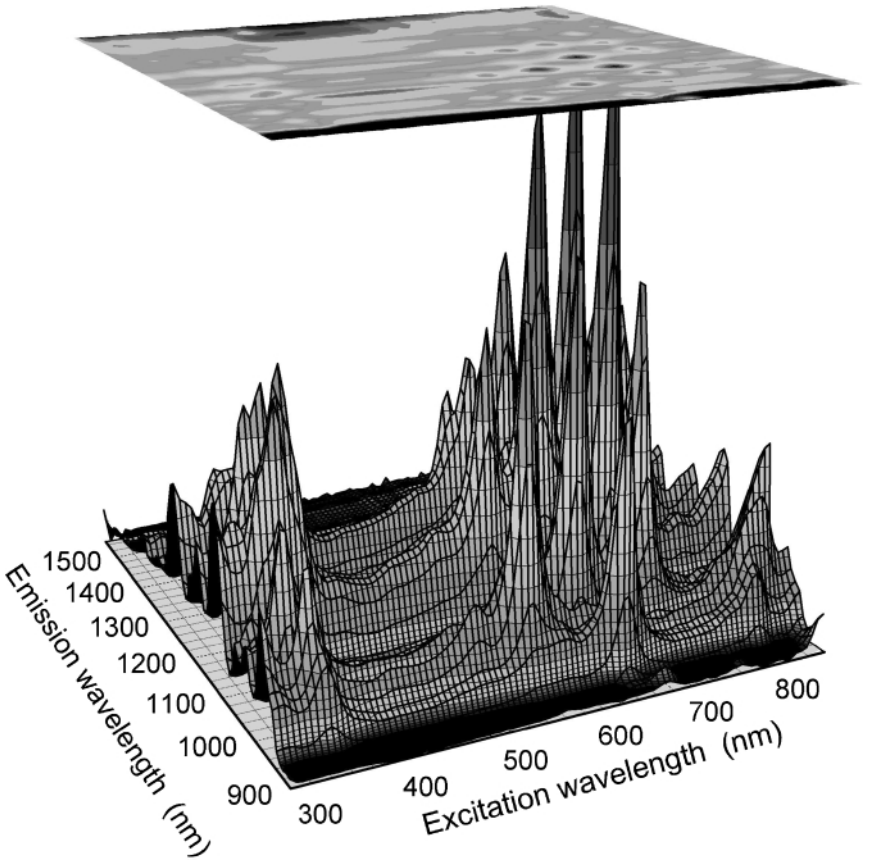

Figure 10 Fluorescence intensity versus excitation and emission wavelengths for SWNTs in an SDS (sodium dodecyl sulfate) suspension (79). Each peak corresponds to absorption/emission of a single (n, m) SWNT.

absorption and photoluminescence data (80–82). Resonance Raman experiments on HiPco bundle samples ($d_t \sim 1.0 \pm 0.3$ nm) (81) and Stokes versus anti-Stokes experiments on isolated SWNTs with diameters smaller than 1 nm (16) show some deviations between experiment and TB theory, the disagreement being more important for smaller diameter SWNTs (d_t below 1.1 nm) owing to the nanotube curvature effect. The experimental values for E_{22}^S were indeed found to be lower than the TB E_{22}^S, but the measured E_{22}^S appear not to be more than 20 meV lower than TB values for SWNTs with diameters down to 0.83 nm (16). However, such an analysis depends on the (n, m) assignment that is usually obtained from the relation between the RBM frequency and the nanotube diameter, and both experimental (16, 61) and ab initio calculations (62) show that such a dependence is not simple for small-diameter SWNTs.

Optical measurements at the single nanotube level also provide precise information about many-body effects, which change the electronic transition energies in semiconducting SWNTs differently for different energy levels. The many-body effects depend on the effective masses of electrons and holes, and the effective masses are energy dependent. The one-electron TB model can account only for an averaged many-body effect, and the value $\gamma_0 = 2.90$ eV can be seen as the best value for an average description of the electronic levels involved in optical absorption and Raman spectroscopy (approximately 1 eV from the Fermi level). However, the γ_0 parameter obtained by transport measurements near the Fermi level, for example, is usually smaller than 2.9 eV (83). The recent optical absorption and emission (photoluminescence) experiments, as in Figure 10, show a considerable change in the E_{11}^S gap energy with respect to TB results used for optical experiments (10). A value of 1.7 for the average ratio of E_{22}^S/E_{11}^S (79) has been reported, which is smaller than the average value of 2.0 predicted by the TB model. [Average values are used because E_{22}^S/E_{11}^S depends on (n, m) at the single nanotube level.] Detailed many-body calculations are in progress to account for these experimental observations (84).

More detailed TB models have been proposed, such as a TB model accounting for up to third-neighbor interactions (85) or considering different wave-function overlaps between the three first-neighbors of a given carbon atom (86). This second model has been shown to give better agreement with the E_{22}^S/E_{11}^S data obtained by optical absorption and photoluminescence experiments (81, 87).

However, inconsistent results were obtained when comparing E_{ii} obtained from different experiments. The experimental results for the various photophysics experiments were developed using samples prepared in different ways and measured under different experimental environments (solutions, substrates, etc.). Fluorescence spectra from individual SWNTs with identical structure were found to exhibit different emission energies and linewidths, and these differences are attributed to defects or differences in local environment (88, 89). Systematic studies using similar samples prepared under similar experimental conditions are necessary for developing a clear model for the photophysics of SWNTs. Experimental results on free-standing SWNTs (90) may provide a good strategy for avoiding environmental effects on these nanometer-sized materials.

Interesting information can be obtained using cross-polarized light or even circularly polarized light in absorption/emission studies, such as in the measurement of the asymmetry between the valence and conduction bands for individual SWNTs with respect to the Fermi level (51) and the chirality handedness (left and right) of carbon nanotubes (91). Experiments with cross-polarized light and circularly polarized light propagating along the nanotube axis directions are, however, technically challenging, in part because optical transitions induced by light polarized perpendicular to the tube axis are much weaker owing to the antenna effect. Although Raman experiments provide evidence for transitions involving cross-polarized light (51), such transitions have not yet been reported in absorption experiments.

SWNTs are also promising for ultra-small optical device applications. For example, induced band-gap luminescence (92) owing to the recombination of electron and hole carriers and photoconductivity (93) have both been observed at the single isolated nanotube level. The research done thus far indicates that many novel and interesting new phenomena can be probed in carbon nanotubes by photophysics studies because, for such nanometer scale systems, the massless light turns out to be the only probe that does not strongly perturb the electronic states of the system. Nevertheless, to gain detailed understanding, systematic experimental and theoretical studies using multiple optical techniques have to be undertaken.

MECHANICAL PROPERTIES OF NANOTUBES

Because the carbon-carbon chemical bond in a graphene layer is probably the strongest chemical bond known in nature, carbon nanotubes are expected to have exceptionally good mechanical properties, with significant potential for applications in the reinforcement of composite materials.

Some of the important parameters characterizing the mechanical properties of carbon nanotubes include their elastic constants, Young's modulus, Poisson ratio, response to deformation in the elastic regime, tensile and compressive strains, yield mechanism and strength at failure, toughness, and buckling when bent. One of the unusual features of nanotubes is that they simultaneously combine widely varying length scales: Their length can be macroscopic, up to millimeters, whereas their diameters are on the nanoscale. Furthermore, for SWNTs, the physical thickness of the nanotube shell (one carbon atom in thickness) is ill-defined (19, 94–96), leading to different definitions of nanotube parameters by different research groups.

The manipulation of nanoscale objects is a difficult and challenging task; however, a number of direct experimental measurements of the Young's modulus Y of nanotubes have appeared in the literature. The first study reporting the measurement of the Young's modulus of MWNTs was based on the correlation of the thermal oscillation amplitude of the free ends of anchored nanotubes as a function of temperature (97). Calculations show that the Young's modulus of isolated SWNTs does not depend much on nanotube diameter or chiral angle and has a value of approximately 1 TPa, corresponding to the asymptotic limit reported for carbon fibers (3), whereas Y for MWNTs decreases somewhat with increasing d_t. It is expected that tensile strength results for different nanotube samples will depend on the concentration of different types of defects, experimental elastic parameters, and synthesis techniques. Despite the very high Young's modulus for carbon nanotubes, atomic force microscopy (AFM) measurements (98) indicate that nanotubes can bend into loops without breaking, testifying to their flexibility, toughness, and capacity for reversible deformation. Small-diameter SWNTs can be elongated by $\sim$30% before breaking (99, 100), and values for the breaking strength of 55 GPa have been reported (101). It is believed that SWNTs accommodate large strains by forming dislocations with a Stone-Wales 5/7/7/5 pair (102)

at the core of the dislocation. On compression, MWNTs show reversible buckling as a mechanism for accommodating large strains. These Stone-Wales defects trigger the fracture of nanotubes (102). Tensile strength experiments performed on MWNTs showed that they break at the outermost layer, with the inner layers being pulled out like a sword from its sheath, and somewhat smaller values for the tensile strength were found for MWNTs (101).

Under bending stress, MWNTs bend by stretching in the outer arc and by compression in the inner arc. For nanotubes with diameters $d_t < 12$ nm, the effective bending modulus was found to have a value of approximately 1 TPa (103). However, for MWNTs of larger diameters, the effective bending modulus drops dramatically to values of approximately 100 GPa. High-resolution transmission electron microscopy (TEM) images of such large-diameter nanotubes reveal rippled or buckling distortions along the inner arc of bent nanotubes (103–105), thus providing a mechanism for strain-relaxation. From these experiments, it is concluded that MWNTs, although difficult to stretch axially, are easy to bend laterally and they can reversibly withstand large lateral distortions.

Determining the actual strength of nanotubes from simulation is a challenging task owing to the widely varying scales involved in fracture, both in the time and length domains. Owing to computational limitations, simulations are normally too short to span the macroscopic timescale relevant in fracture experiments. Atomistic calculations indicate that chiral tubes have a lower yield strain than either zigzag or armchair nanotubes (106).

THERMAL PROPERTIES

Although the thermal properties of carbon nanotubes, including their specific heat, thermal conductivity, and thermopower, are quite special (19), the thermal properties of SWNTs have not been as extensively studied as the electronic, mechanical, or phonon properties of SWNTs, in part because the techniques for making such studies are still under development (107–110). The thermal properties of carbon nanotubes display a wide range of behaviors that stem from their relation to the corresponding properties of a two-dimensional graphene layer and from their unique structure and tiny size.

At high temperatures, the specific heat of individual nanotubes should be similar to that of two-dimensional graphene, with the effects of phonon quantization becoming apparent at lower temperatures for SWNTs of small diameter (<2 nm), where a linear T dependence of the specific heat is expected. The excitation of specific low-frequency optical phonon modes is expected to be observable as anomalies in the temperature dependence of the specific heat. To study the intrinsic thermal conductivity and thermoelectric power of nanotubes, measurements must be made at the single nanotube level. Such measurements are technically very difficult to make. Therefore, work in this area is just beginning to appear in the literature.

The thermal conductivity of graphite is generally dominated by phonons and is limited by the small crystallite size within a sample. The apparent long-range crystallinity of nanotubes and long phonon mean free path led to the speculation that nanotubes would behave like a heat pipe (104) with a longitudinal thermal conductivity that could possibly exceed the in-plane thermal conductivity of graphite, which, together with diamond, has the highest thermal conductivity of known materials. The reason for the very high thermal conductivity follows from the very high velocity of sound on the basis of kinetic theory arguments and relates to the very high Young's modulus of carbon nanotubes (as discussed above). Measurements of the temperature-dependent thermal conductivity $\kappa(T)$ for an individual MWNT (14 nm diameter) (111) show very high values of κ (more than 3000 W/mK), but only comparable to graphite (in-plane). It is believed that smaller diameter tubes (probably individual SWNTs) will be needed to exhibit thermal conductivities greater than that of graphite. For the 14-nm-diameter MWNT that was measured, the maximum in $\kappa(T)$ at room temperature is indicative of significant phonon-phonon scattering. Furthermore, the slope of 2.0 at low T for a log-log plot of $\kappa(T)$ versus T indicates that a 14-nm MWNT still behaves like a two-dimensional system. The small diameter of SWNTs causes phonon quantization, which should be observable in the heat capacity and in the thermal conductivity at low T. The restricted geometry of the nanotubes suppresses the peak in the thermal conductivity and moves it to higher temperatures compared with graphite, reflecting the fact that phonon-phonon scattering should be suppressed in a one-dimensional system because of the unavailability of states into which to scatter (112, 113). This effect has already been observed in the 14-nm MWNT measurements (111).

The thermal expansion of a SWNT bundle has been measured using X-ray diffraction techniques (114), and the results are consistent with expectations based on graphite, which has an exceedingly small in-plane thermal expansion coefficient but a large inter-planar expansion coefficient. The measurements show almost no thermal expansion along the nanotube axis ($-0.15 \pm 0.20 \times 10^{-5}$/K) direction, but a value of $0.75 \pm 0.25 \times 10^{-5}$/K is found for the expansion along the SWNT diameter direction in the temperature range 300–950 K. The value for the temperature dependence of the intertube gap is $4.2 \pm 1.4 \times 10^{-5}$/K for a SWNT bundle, which is larger than $2.6 \pm 1.4 \times 10^{-5}$/K for graphite, with a significantly larger anharmonicity shown for SWNTs relative to graphite. The very tiny thermal expansion coefficient of the tube diameter reflects the strong in-plane C–C bonds in nanotubes.

Thermopower (TEP) measurements have been of substantial interest to nanotube research. Most TEP measurements have been done on SWNT bundles with random orientations leading to phenomena dominated by intertube interactions, rather than the intrinsic behavior of individual SWNTs. Much attention has focused on the sensitivity of the TEP to exposure to oxygen and other gaseous species (115, 116) because oxygen adsorption causes SWNTs to become p-type and to yield quite high TEP values. This high sensitivity of the TEP to gas adsorption has potential for use as a gas sensor (117). However, for quantitative measurements of

the *T* dependence of the intrinsic TEP of SWNTs, the removal of adsorbed gases is essential because the thermopower is sensitive to charge transfer effects and to the motion of the Fermi level, which can potentially be used to characterize SWNTs. TEP measurements on individual SWNT bundles and individual SWNTs are now in progress. By measuring the TEP and electrical conductance at the same time, detailed studies of low-temperature universal conductance fluctuations and Coulomb blockade phenomena were carried out by P. Kim (private communication). The results show that the TEP follows in detail the universal conductance fluctuations observed in the conductance, in accordance with the Mott formula. The effects of the Coulomb blockade and of electron-electron interaction can be seen in metallic SWNTs. The TEP of semiconducting SWNTs appears to be qualitatively different from that for metallic SWNTs (P. Kim, private communication).

Thermal measurements at the individual nanotube level are expected to have a major impact on the direction of future studies on the thermal properties of nanotubes, allowing more detailed measurements of intertube contributions to the thermal conductivity and to the TEP, the tube diameter dependence of various thermal processes, differences in behavior of thermal processes in semiconducting and metallic SWNTs, the role of optical phonons in thermal processes, and the effect of specific adsorbed gases and dopants on the thermal and thermoelectric properties of nanotubes. The study of quantum thermal phenomena at low temperatures should be especially interesting regarding studies of the effect of individual selected phonons on thermal properties.

FILLED TUBES AND DOUBLE-WALL NANOTUBES

A remarkable property of nanotubes is the possibility of filling their hollow cores with guest species to generate very-small-diameter one-dimensional quantum wires embedded within a carbon nanotube shell. The spatial confinement of these quantum wires often leads to crystalline arrangements not found in the bulk (118). One particularly interesting quantum wire thus formed comes from filling a SWNT with a linear array of C_{60} fullerene molecules to form what is called a peapod (119–122).

The filling of nanotubes is usually accomplished by using a mild acid to open the nanotube ends and to fill the inner core of the nanotube with metals or with molecular species by exploiting the capillary properties of nanotubes (123) or a charge transfer mechanism. Thus, the hollow cores of nanotubes provide a host material for the synthesis of many new and novel materials. This research is still at an early stage, although many novel materials have already been synthesized and their structures have been identified by high-resolution transmission electron microscopy (HRTEM) studies (118). Raman spectroscopy has also provided a powerful tool for studying the electronic and vibrational properties of nanotubes filled with C_{60} and other organic species (124, 125).

Of all these systems, the C_{60} peapods have been the most extensively studied (119–122), in part because when annealed in vacuum to temperatures of $\sim$1200°C,

the C_{60} molecules within the hollow core of the SWNT are transformed into an inner tube to form a DWNT, as investigated in some detail using joint systematic HRTEM and Raman spectroscopy with several different laser excitation energies (124, 126). Because of different nanotube diameters of the inner and outer tubes of the DWNTs and the relatively weak coupling between tubes, the radial breathing mode spectra from the inner tubes can be observed separately from those from the outer tubes (see Section 5, above). Of particular significance is the very sharp Raman features (less than 1 cm^{-1} linewidth) observed for the inner tube of the DWNTs, showing that the intertube interactions are very weak and that the hollow core of a nanotube provides an ideal environment for studying the vibrational spectra for nanotubes in the quantum limit (127).

DWNTs are especially interesting for detailed studies of tube-tube interactions because of the possibility of carrying out studies of the individual constituents of the DWNTs at the single nanotube level. Thus, DWNTs can be considered as model systems for understanding the more complex behavior of MWNTs, which are likely to be used in a variety of applications requiring more rugged performance than SWNTs can provide.

CONCLUDING REMARKS

The field of carbon nanotube research is remarkable in terms of the unique physical properties of the carbon nanotubes, some of which are reviewed in this chapter. In most subfields of condensed matter physics, experimental results have led the way and theoretical explanations have followed to give the subfield a firm foundation. However, in the case of research on carbon nanotubes, theoretical predictions have often led experimental investigations. This situation is directly related to the difficulty in synthesis of sufficient quantities of pure and well-characterized materials for detailed, systematic experimental investigations and to the fundamental nature of SWNTs as an attractive prototype system for the theoretical investigation of one-dimensional phenomena.

Although extensive experimental study of carbon nanotubes is quite recent, progress in the experimental aspects of this field since 1996 has been rapid, encouraging theorists to develop more sophisticated models regarding all aspects of carbon nanotube behavior. Despite this rapid progress, the field is still at a relatively early stage of development, from both an experimental and theoretical standpoint. Thus, in writing this review article, the authors have attempted to focus on those models and measurements that are likely to stand the test of time and will help to guide future developments in this field.

Currently, it is not clear whether the applications of carbon nanotubes will be sufficient to ensure long-term interest in carbon nanotube–based materials. Because of the unique properties of SWNTs there are great expectations that practical applications will eventually be developed. However, because of their use as a prototype one-dimensional materials system for theoretical and experimental

studies, it is likely that scientific interest in carbon nanotubes will continue to be a focus of materials research for some time into the future.

ACKNOWLEDGMENTS

M.S.D. and G.D. gratefully acknowledge support from NSF grant DMR01-16042, and A.J. acknowledges financial support from PRPq–UFMG and CNPq, Brazil. The authors also acknowledge stimulating discussions with Profs. J.-C. Charlier and M.A. Pimenta.

LITERATURE CITED

1. Endo M. 1975. *Mecanisme de croissance en phase vapeur de fibres de carbone*. PhD thesis. Univ. Orleans, France (In French)
2. Iijima S. 1991. Helical microtubules of graphitic carbon. *Nature* 354:56–58
3. Dresselhaus MS, Dresselhaus G, Sugihara K, Spain IL, Goldberg HA. 1988. *Graphite Fibers and Filaments*, Vol. 5. *Springer Ser. Mater. Sci*. Berlin: Springer-Verlag
4. Saito R, Fujita M, Dresselhaus G, Dresselhaus MS. 1992. Electronic structures of carbon fibers based on C_{60}. *Phys. Rev. B* 46:1804–11
5. Mintmire JW, Dunlap BI, White CT. 1992. Are fullerene tubules metallic? *Phys. Rev. Lett*. 68:631–34
6. Hamada N, Sawada S, Oshiyama A. 1992. New one-dimensional conductors: graphitic microtubules. *Phys. Rev. Lett*. 68:1579–81
7. Iijima S, Ichihashi T. 1993. Single shell carbon nanotubes of 1-nm diameter. *Nature* 363:603
8. Bethune DS, Kiang CH, de Vries MS, Gorman G, Savoy R, et al. 1993. Cobalt-catalysed growth of carbon nanotubes with single atomic layer walls. *Nature* 363:605
9. Thess A, Lee R, Nikolaev P, Dai H, Petit P, et al. 1996. Crystalline ropes of metallic carbon nanotubes. *Science* 273:483–87
10. Saito R, Dresselhaus G, Dresselhaus MS. 1998. In *Physical Properties of Carbon Nanotubes*. London: Imp. Coll. Press
11. Dresselhaus MS, Dresselhaus G, Eklund PC. 1996. *Science of Fullerenes and Carbon Nanotubes*. New York/San Diego: Academic
12. Dresselhaus MS, Dresselhaus G, Saito R. 1992. Carbon fibers based on C_{60} and their symmetry. *Phys. Rev. B* 45:6234
13. Saito R, Fujita M, Dresselhaus G, Dresselhaus MS. 1992. Electronic structure of chiral graphene tubules. *Appl. Phys. Lett*. 60:2204–6
14. Tans SJ, Devoret MH, Dai H, Thess A, Smalley RE, et al. 1997. Individual single-wall carbon nanotubes as quantum wires. *Nature* 386:474–77
15. Samsonidze GG, Saito R, Jorio A, Pimenta MA, Souza Filho AG, et al. 2003. The concept of cutting lines in carbon nanotube science. *J. Nanosci. Nanotechnol*. 3:431
16. Souza Filho AG, Chou SG, Samsonidze GG, Dresselhaus G, Dresselhaus MS, et al. 2004. Stokes and anti-Stokes Raman spectra of small diameter isolated carbon nanotubes. *Phys. Rev. B* 69:1154XX
17. Chico L, Crespi VH, Benedict LX, Louie SG, Cohen ML. 1996. Pure carbon nanoscale devices: nanotube heterojunctions. *Phys. Rev. Lett*. 76:971–74

18. Blase X, Benedict LX, Shirley EL, Louie SG. 1994. Hybridization effects and metallicity in small radius carbon nanotubes. *Phys. Rev. Lett.* 72:1878
19. Dresselhaus MS, Dresselhaus G, Charlier JC, Hernández E. 2004. Electronic, thermal and mechanical properties of carbon nanotubes. *Philos. Trans. R. Soc.* In press
20. Liu HJ, Chan CT. 2002. Properties of 4 Å carbon nanotubes from first-principles calculations. *Phys. Rev. B* 66:115416
21. Cabria I, Mintmire JW, White CT. 2003. Metallic and semiconducting narrow carbon nanotubes. *Phys. Rev. B* 67:121406
22. Wang N, Tang ZK, Li GD, Chen JS. 2000. Single-walled 4 Å carbon nanotube arrays. *Nature* 408:50
23. Tang ZK, Zhang L, Wang N, Zhang XX, Wen GH, et al. 2001. Superconductivity in 4 Å SWNTs. *Science* 292:2462–65
24. Liu BB, Sundqvist B, Li DM, Zou GT. 2002. Resistivity and fractal structure in carbon nanotube networks. *J. Phys.-Condens. Matter* 44:11125–29
25. Sanchez-Portal D, Artacho E, Soler JM, Rubio A, Ordejón P. 1999. Ab initio structural, elastic, and vibrational properties of carbon nanotubes. *Phys. Rev. B* 59:12678–88
26. Bockrath M, Cobden DH, McEuen PL, Chopra NG, Zettl A, et al. 1997. Single-electron transport in ropes of carbon nanotubes. *Science* 275:1922–25
27. Langer L, Bayot V, Grivei E, Issi JP, Heremans JP, et al. 1996. Quantum transport in a multiwalled carbon nanotube. *Phys. Rev. Lett.* 76:479–82
28. Ebbesen TW, Lezec HJ, Hiura H, Bennett JW, Ghaemi HF, Thio T. 1996. Electrical conductivity of individual carbon nanotubes. *Nature* 382:54–56
29. Dai H, Wong EW, Lieber CM. 1996. Probing electrical transport in nanomaterials: conductivity of individual carbon nanotubes. *Science* 272:523–26
30. Wildöer JWG, Venema LC, Rinzler AG, Smalley RE, Dekker C. 1998. Electronic structure of carbon nanotubes investigated by scanning tunneling spectroscopy. *Nature* 391:59–62
31. Odom TW, Huang JL, Kim P, Lieber CM. 1998. Atomic structure and electronic properties of single-walled carbon nanotubes. *Nature* 391:62–64
32. Dunlap BI. 1994. Relating carbon tubules. *Phys. Rev. B* 49:5643–51
33. Lambin P, Fonseca A, Vigneron JP, Nagy JB, Lucas AA. 1995. Structural and electronic properties of bent carbon nanotubes. *Chem. Phys. Lett.* 245:85–89
34. Saito R, Dresselhaus G, Dresselhaus MS. 1996. Tunneling conductance of connected carbon nanotubes. *Phys. Rev. B* 53:2044–50
35. Charlier JC, Ebbesen TW, Lambin P. 1996. Structural and electronic properties of pentagon-heptagon pair defects in carbon nanotubes. *Phys. Rev. B* 53:11108
36. Yao Z, Postma HWC, Balents L, Dekker C. 1999. Carbon nanotube intramolecular junctions. *Nature* 402:273
37. Ouyang M, Huan JL, Cheung CL, Lieber CM. 2001. When are metallic SWNTs metals? *Science* 292:702
38. Terrones M, Terrones G, Terrones H. 2002. Structure, chirality and formation of giant icosahedral fullerenes and spherical graphitic onions. *Appl. Phys. A Matter* 74:355–71
39. Terrones M, Banhart F, Grobert N, Charlier JC, Terrones H, Ajayan PM. 2002. Molecular junctions by joining SWNTs. *Phys. Rev. Lett.* 89:075505
40. Derycke V, Martel R, Appenzeller J, Avouris P. 2001. Carbon nanotube inter- and intra-molecular logic gates. *Nano Lett.* 1:453
41. Björk MT, Ohlsson BJ, Thelander C, Persson AI, Deppert K, et al. 2001. Nanowire resonant tunneling diodes. *Appl. Phys. Lett.* 21(23):4458–60
42. Bachtold A, Hadley P, Nakanishi T, Dekker C. 2001. Logic circuits with carbon nanotube transistors. *Science* 294: 1317–20

43. Jorio A, Pimenta MA, Souza Filho AG, Saito R, Dresselhaus G, Dresselhaus MS. 2003. Characterizing carbon nanotube samples with resonance Raman scattering. *New J. Phys.* 5:139
44. Dresselhaus MS, Eklund PC. 2000. Phonons in carbon nanotubes. *Adv. Phys.* 49:705–814
45. Rao AM, Richter E, Bandow S, Chase B, Eklund PC, et al. 1997. Diameter-selective Raman scattering from vibrational modes in carbon nanotubes. *Science* 275:187–91
46. Dresselhaus MS, Dresselhaus G, Rao AM, Jorio A, Souza Filho AG, et al. 2003. Resonant Raman scattering on one-dimensional systems. *Indian J. Phys.* 77B: 75–99
47. Jorio A, Saito R, Hafner JH, Lieber CM, Hunter M, et al. 2001. Structural (n, m) determination of isolated single-wall carbon nanotubes by resonant Raman scattering. *Phys. Rev. Lett.* 86:1118–21
48. Pimenta MA, Marucci A, Empedocles S, Bawendi M, Hanlon EB, et al. 1998. Raman modes of metallic carbon nanotubes. *Phys. Rev. B* 58:R16016–19
49. Brown SDM, Jorio A, Corio P, Dresselhaus MS, Dresselhaus G, et al. 2001. Origin of the Breit–Wigner–Fano lineshape of the tangential G-band feature of metallic carbon nanotubes. *Phys. Rev. B* 63:155414
50. Jorio A, Dresselhaus G, Dresselhaus MS, Souza M, Dantas MSS, et al. 2000. Polarized Raman study of single-wall semiconducting carbon nanotubes. *Phys. Rev. Lett.* 85:2617–20
51. Jorio A, Pimenta MA, Souza Filho AG, Samsonidze GG, Swan AK, et al. 2003. Resonance Raman spectra of carbon nanotubes by cross-polarized light. *Phys. Rev. Lett.* 90:107403
52. Thomsen C, Reich S. 2000. Double resonant Raman scattering in graphite. *Phys. Rev. Lett.* 85:5214
53. Souza Filho AG, Jorio A, Samsonidze GG, Dresselhaus G, Dresselhaus MS, et al. 2002. Probing the electronic trigonal warping effect in individual single-wall carbon nanotubes using phonon spectra. *Chem. Phys. Lett.* 354:62–68
54. Saito R, Dresselhaus G, Dresselhaus MS. 2000. Trigonal warping effect of carbon nanotubes. *Phys. Rev. B* 61:2981–90
55. Samsonidze GG, Saito R, Jorio A, Souza Filho AG, Grüneis A, et al. 2003. Phonon trigonal warping effect in graphite and carbon nanotubes. *Phys. Rev. Lett.* 90:027403
56. Brar VW, Samsonidze GG, Dresselhaus G, Dresselhaus MS, Saito R, et al. 2002. Second-order harmonic and combination modes in graphite, single-wall carbon nanotube bundles, and isolated single-wall carbon nanotubes. *Phys. Rev. B* 66: 155418
57. Deleted in proof
58. Kataura H, Kumazawa Y, Maniwa Y, Umezu I, Suzuki S, et al. 1999. Optical properties of single-wall carbon nanotubes. *Synth. Met.* 103:2555–58
59. Dresselhaus G, Pimenta MA, Saito R, Charlier JC, Brown SDM, et al. 1999. On the π–π overlap energy in carbon nanotubes. In *Science and Applications of Nanotubes*, ed. D Tománek, RJ Enbody, pp. 275–95. New York: Kluwer Acad.
60. Dresselhaus MS, Dresselhaus G, Jorio A, Souza Filho AG, Saito R. 2002. Raman spectroscopy on isolated single wall carbon nanotubes. *Carbon* 40:2043–61
61. Kuzmany H, Plank W, Hulman M, Kramberger C, Grüneis A, et al. 2001. Determination of SWCNT diameters from the Raman response of the radial breathing mode. *Eur. Phys. J. B* 22:307–20
62. Kürti J, Zólyomi V, Kertesz M, Sun GY. 2003. The geometry and the radial breathing mode of carbon nanotubes: beyond the ideal behaviour. *New J. Phys.* 5: 125
63. Thomsen C, Reich S. 2000. Double resonant Raman scattering in graphite. *Phys. Rev. Lett.* 85:5214

64. Kürti J, Zólyomi V, Grüneis A, Kuzmany H. 2002. Double resonant Raman phenomena enhanced by van Hove singularities in single-wall carbon nanotubes. *Phys. Rev. B* 65:165433
65. Souza Filho AG, Jorio A, Swan AK, Ünlü MS, Goldberg BB, et al. 2002. Anomalous two-peak *G′*-band Raman effect in one isolated single-wall carbon nanotube. *Phys. Rev. B* 65:085417
66. Souza Filho AG, Jorio A, Dresselhaus G, Dresselhaus MS, Saito R, et al. 2002. Effect of quantized electronic states on the dispersive Raman features in individual single wall carbon nanotubes. *Phys. Rev. B* 65:035404
67. Souza Filho AG, Jorio A, Samsonidze GG, Dresselhaus G, Saito R, Dresselhaus MS. 2003. Raman spectroscopy for probing chemically/physically induced phenomena in carbon nanotubes. *Nanotechnology* 14:1130–39. http://stacks.iop.org/0957-4484/14/1130
68. Cronin SB, Chou SG, Rabin O, Dresselhaus MS, Swan AK, et al. 2004. Electrochemical gating of individual carbon SWNTs observed by transport measurements and resonant confocal micro-Raman spectroscopy. *Appl. Phys. Lett.* In press
69. Deleted in proof
70. Jorio A, Souza Filho AG, Dresselhaus G, Dresselhaus MS, Saito R, et al. 2001. Joint density of electronic states for one isolated single-wall carbon nanotube studied by resonant Raman scattering. *Phys. Rev. B* 63:245416
71. Saito R, Jorio A, Souza Filho AG, Dresselhaus G, Dresselhaus MS, Pimenta MA. 2002. Probing phonon dispersion relations of graphite by double resonance Raman scattering. *Phys. Rev. Lett.* 88:027401
72. Nicklow R, Wakabayashi N, Smith HG. 1972. Lattice dynamics of pyrolytic graphite. *Phys. Rev. B* 5:4951–62
73. Niyogi S, Hamon MA, Hu H, Zhao B, Bhowmik P, et al. 2002. Chemistry of single-walled carbon nanotubes. *Acc. Chem. Res.* 35:1105–13
74. Ugawa A, Rinzler AG, Tanner DB. 1999. Far-infrared gaps in single-wall carbon nanotubes. *Phys. Rev. B* 60:R11305
75. Hertel T, Moos G. 2000. Influence of excited electron lifetimes on the electronic structure of carbon nanotubes. *Chem. Phys. Lett.* 320:359–64
76. Moos G, Fasel R, Hertel T. 2003. Temperature dependence of electron-to-lattice energy transfer in single-wall carbon nanotube bundles. *J. Nanosci. Nanotech.* 3: 145–49
77. Hertel T, Moos G. 2000. Electron-phonon interaction in single-wall carbon nanotubes: a time-domain study. *Phys. Rev. Lett.* 84:5002–5
78. Dresselhaus MS, Dresselhaus G, Jorio A, Souza Filho AG, Samsonidze GG, Saito R. 2003. Science and applications of single nanotube Raman spectroscopy. *J. Nanosci. Nanotech.* 3:19–37
79. O'Connell MJ, Bachilo SM, Huffman XB, Moore VC, Strano MS, et al. 2002. Band gap fluorescence from individual single walled carbon nanotubes. *Science* 297:593–96
80. Bachilo SM, Strano MS, Kittrell C, Hauge RH, Smalley RE, Weisman RB. 2002. Structure-assigned optical spectra of single walled carbon nanotubes. *Science* 298:2361–66
81. Hagen A, Hertel T. 2003. Quantitative analysis of optical spectra from individual single-wall carbon nanotubes. *Nanoletters* 3:383–88
82. Weisman RB, Bachilo SM. 2003. Dependence of optical transition energies on structure for single-walled carbon nanotubes in aqueous suspension: an empirical Kataura plot. *Nanoletters* 3:1235–38
83. Dresselhaus MS, Dresselhaus G, Avouris P. 2001. *Carbon Nanotubes: Synthesis, Structure, Properties and Applications. Topics Appl. Phys.* Vol. 80. Berlin: Springer-Verlag

84. Kane CL, Mele EJ. 2003. Ratio problem in single nanotube fluorescence spectroscopy. *Phys. Rev. Lett.* 90:207401
85. Reich S, Maultzsch J, Thomsen C, Ordejón P. 2002. Tight-binding description of graphene. *Phys. Rev. B* 66:035412
86. Ding JW, Yan XH, Cao JX. 2002. Analytical relation of band gaps to both chirality and diameter of single-wall carbon nanotubes. *Phys. Rev. B* 66:073401
87. Lebedkin S, Arnold K, Hennrich F, Krupke R, Renker B, Kappes MM. 2003. FTIR-luminescence mapping of dispersed single-walled carbon nanotubes. *New J. Phys.* 5:140
88. Hartschuh A, Pedrosa HN, Novotny L, Krauss TD. 2003. Simultaneous fluorescence and Raman scattering from single carbon nanotubes. *Science* 301:1354–56
89. Hartschuh A, Sanchez EJ, Xie XS, Novotny L. 2003. High-resolution near-field Raman microscopy of single-walled carbon nanotubes. *Phys. Rev. Lett.* 90: 95503
90. Lefebvre J, Homma Y, Finnie P. 2003. Bright band gap photoluminescence from unprocessed single-wall carbon nanotubes. *Phys. Rev. Lett.* 90:217401
91. Samsonidze GG, Grüneis A, Saito R, Jorio A, Souza Filho AG, et al. 2004. Interband optical transitions in left and right handed single wall carbon nanotubes. *Phys. Rev. B*. In press
92. Misewich JA, Martel R, Avouris P, Tsang JC, Heinze S, Tersoff J. 2003. Electrically induced optical emission from a carbon nanotube FET. *Science* 300:783–86
93. Freitag M, Martin Y, Misewich JA, Martel R, Avouris P. 2003. Photoconductivity of single carbon nanotubes. *Nanoletters* 3:1067–71
94. Hernández E, Goze C, Bernier B, Rubio A. 1998. Elastic properties of C and $B_xC_yN_z$ composite nanotubes. *Phys. Rev. Lett.* 80:4502–5
95. Hernández E, Goze C, Bernier P, Rubio A. 1999. Elastic properties of single-wall nanotubes. *Appl. Phys. A* 68:287–92
96. Yakobson BI, Avouris P. 2001. Mechanical properties of carbon nanotubes. See Ref. 83, pp. 287–327
97. Treacy MMJ, Ebbesen TW, Gibson JM. 1996. Exceptionally high Young's modulus observed for individual carbon nanotubes. *Nature* 381:678
98. Falvo MR, Clary GJ, Taylor RM II, Chi V, Brooks FP Jr, et al. 1997. Bending and buckling of carbon nanotubes under large strain. *Nature* 389:582–84
99. Yakobson BI, Smalley RE. 1997. Fullerene nanotubes: $C_{1,000,000}$ and beyond. *Am. Sci.* 85:324
100. Yakobson BI. 1998. Mechanical relaxation and intramolecular plasticity in carbon nanotubes. *Appl. Phys. Lett.* 72:918
101. Yu MF, Files BS, Arepalli S, Ruoff RS. 2000. Tensile loading of ropes of single-wall carbon nanotubes and their mechanical properties. *Phys. Rev. Lett.* 84:5552–55
102. Nardelli MB, Yakobson BI, Bernholc J. 1998. Brittle and ductile behavior in carbon nanotubes. *Phys. Rev. Lett.* 81:4656
103. Poncharal P, Wang ZL, Ugarte D, de Heer WA. 1999. Electrostatic deflections and electromechanical resonances of carbon nanotubes. *Science* 283:1513–16
104. Ruoff RS, Lorents DC. 1995. Mechanical and thermal properties of carbon nanotubes. *Carbon* 33:925
105. Lourie O, Wagner HD. 1998. Evaluation of Young's modulus of carbon nanotubes by micro-Raman spectroscopy. *J. Mater. Res.* 13:2418
106. Samsonidze GG, Samsonidze GG, Yakobson BI. 2002. Kinetic theory of symmetry-dependent strength in carbon nanotubes. *Phys. Rev. Lett.* 88:065501
107. Majumdar A. 1999. Thermal transport measurements of individual multiwalled nanotubes. *Annu. Rev. Mater. Sci.* 29:505–85
108. Fan X, Zeng G, LaBounty C, Bowers J, Croke E, et al. 2001. SiGeC/Si superlattice

microcoolers. *Appl. Phys. Lett.* 78:1580–82

109. Majumdar A. 2004. Thermoelectricity in semiconductor nanostructures. *Science* 303:777–78 223
110. Huxtable ST, Abramson AR, Majumdar A. 2003. Heat transport in superlattices and nanowires. In *Heat and Fluid Flow in Microscale and Nanoscale Structures*, ed. M Faghri, B Sunden. Southampton, UK: WIT Press. 392 pp.
111. Small JP, Shi L, Kim P. 2003. Mesoscopic thermal and thermoelectric measurements of individual carbon nanotubes. *Solid State Commun.* 127:181–86
112. Peierls R. 1995. *Quantum Theory of Solids*. Oxford, UK: Oxford Univ. Press
113. Jishi RA, Dresselhaus MS, Dresselhaus G, Wang K, Zhou P, et al. 1993. Vibrational mode frequencies in C_{70}. *Chem. Phys. Lett.* 206:187–92
114. Maniwa Y, Fujiwara R, Kira H, Kataura H, Suzuki S, et al. 2001. Thermal expansion of swnt bundles: X-ray diffraction studies. *Phys. Rev. B* 64:2424029R
115. Sumanasekera GU, Adu CKW, Fang S, Eklund PC. 2000. Effects of gas adsorption and collisions on electrical transport in single-walled carbon nanotubes. *Phys. Rev. Lett.* 85:1096
116. Sumanasekera GU, Pradhan BK, Romero HE, Adu CKW, Eklund PC. 2002. Giant thermopower effects from molecular physisorption on carbon nanotubes. *Phys. Rev. Lett.* 89:166801
117. Sumanasekera GU, Pradhan BK, Adu CKW, Romero HE, Foley HC, Eklund PC. 2002. Thermoelectric chemical sensor based on single wall carbon nanotubes. *Mol. Cryst. Liq. Cryst. Sci. Technol. A* 387:31
118. Sloan J, Kirk AI, Hutchison JL, Green MLH. 2002. Structural characterization of atomically regulated nanocrystals formed within single-walled carbon nanotubes using electron microscopy. *Acc. Chem. Res.* 35:1054–62
119. Smith BW, Monthioux M, Luzzi DE. 1998. Encapsulated C_{60} in carbon nanotubes. *Nature* 396:323–24
120. Luzzi DE, Smith BW. 2000. Carbon cage structures in single wall carbon nanotubes: a new class of materials. *Carbon* 38:1751–56
121. Vavro J, Llaguno MC, Satishkumar BC, Luzzi DE, Fischer JE. 2002. Electrical and thermal properties of C_{60}-filled single-wall carbon nanotubes. *Appl. Phys. Lett.* 80:1450–52
122. Hornbaker DJ, Kahng SJ, Misra S, Smith BW, Johnson AT, et al. 2002. Mapping the one-dimensional electronic states of nanotube peapod structures. *Science* 295:828–31
123. Ajayan PM, Ebbesen TW, Ichihashi T, Iijima S, Tanigaki K, Hiura H. 1993. Opening carbon nanotubes with oxygen and implications for filling. *Nature* 362: 522
124. Bandow S, Takizawa M, Hirahara K, Yudasaka M, Iijima S. 2001. Raman scattering study of double-wall carbon nanotubes derived from the chains of fullerenes in single-wall carbon nanotubes. *Chem. Phys. Lett.* 337:48–54
125. Takenobu T, Takano T, Shiraishi M, Murakami Y, Shiraishi M, et al. 2003. Stable and controlled amphoteric doping by encapsulation of organic molecules inside carbon nanotubes. *Nat. Mater.* 2:683–88
126. Bandow S, Chen G, Sumanasekera GU, Gupta R, Yudasaka M, et al. 2002. Diameter-selective resonant Raman scattering in double-wall carbon nanotubes. *Phys. Rev. B* 66:075416
127. Pfeiffer R, Kuzmany H, Schaman C, Pichler T, Kataura HA et al. 2003. Unusual high degree of unperturbed environment in the interior of single-wall carbon nanotubes. *Phys. Rev. Lett.* 90:225501

Annual Review of Materials Research
Volume 34, 2004

CONTENTS